AIMS Mathematics, 11(1): 785–809.
DOI:10.3934/math.2026034
Received: 31 October 2025
Revised: 20 December 2025
Accepted: 06 January 2026
Published: 12 January 2026

https://www.aimspress.com/journal/Math

Research article

Persistent homology via curvature-adaptive wing complexes

Zishan Weng and Minghui Zhao*

School of Science, Beijing Forestry University, Beijing 100083, China

* **Correspondence:** Email: zhaomh@bjfu.edu.cn.

Abstract: Persistent homology is a key tool in topological data analysis, used to capture the topological features of data across multiple scales. To accurately capture the topology of data with varying geometric structures, one should construct suitable simplicial complexes. In this paper, we propose wing complexes as a novel method for finite sets of points sampled from a smooth plane curve. The key innovation of the wing complex lies in its ability to stretch and shrink along the tangent and normal directions based on a specific parameter, allowing it to adapt to the local curvature variations of the data. We theoretically derive the topological properties of wing complexes and conduct related experiments. The results demonstrate that, compared to traditional methods, wing complexes provide more persistent and accurate topological features, particularly in regions with rapid local curvature variations, whereas traditional methods often fail to capture the correct topological features.

Keywords: persistent homology; topological data analysis; simplicial complexes; wing complexes; topological properties
Mathematics Subject Classification: 55N31, 68T09

1. Introduction

Persistent homology is one of the most important tools in topological data analysis [1, 2]. It tracks the evolution of topological features across multiple scales, effectively extracting the topological features with significant persistence from the underlying structure of the data [3, 4]. Compared to traditional methods, the advantage of persistent homology lies in its low dependence on specific coordinates or metric information of the data [5, 6], which has led to its widespread attention. In practical applications, persistent homology has been successfully applied in various fields, including chemistry [7], medicine [8], and genomics [9]. In shape segmentation, Liu et al. proposed a topology-aware segmentation module that imposes topological constraints on the segmentation of 3D point clouds, thereby improving the performance of point cloud segmentation tasks [10]. He et al. introduced persistent homology into the analysis of a fractional-order delay financial risk system. By capturing the

dynamic evolution of the financial risk system from a topological perspective, this approach provides new insights for financial regulation [11]. Moreover, persistent homology can be effectively combined with deep learning frameworks, thereby improving the accuracy and efficiency of traditional analytical methods [12]. For an in-depth introduction to persistent homology, see [13–15].

In persistent homology, constructing a simplicial complex is a key step in approximating the underlying shape of a dataset. For unstructured data in the form of a point cloud, a common approach is to build the Čech complex or the Vietoris–Rips complex [16, 17]. The persistent homology algorithms based on Čech complexes and Vietoris–Rips complexes have been well developed and are supported by numerous libraries that are readily available for use [18, 19], making them highly effective for most types of datasets. Moreover, for large-scale or high-dimensional point cloud data, alternative constructions such as alpha complexes and witness complexes have been proposed to accelerate persistent homology computations by reducing the size of the simplicial complex while preserving essential topological information [20, 21].

However, in practical computations, when dealing with underlying spaces that are manifolds or have bottlenecks (see Subsection 2.1.2), using isotropic balls centered at sample points may cause premature connections in the bottleneck regions, resulting in the capture of incorrect topological structures in the original data [22]. In fact, for such data, simplicial complexes that adapt to curvature variations offer a more accurate fit. In 2024, Kališnik et al. introduced ellipsoid complexes, which are composed of a set of ellipsoids that can stretch along tangent directions [23, 24]. Compared to Čech complexes and Vietoris–Rips complexes, ellipsoid complexes can capture more persistent topological features when applied to such data.

In this paper, we introduce wing complexes for finite sets of points sampled from a smooth plane curve. First, we formally define the wing complex for general point clouds and explain its construction. Second, we reveal the relationship between wing complexes and their angular parameters, derive certain topological properties of wing complexes, and provide rigorous proofs. Finally, we compare wing complexes with Rips complexes through experimental analysis. The experiments show that, when dealing with certain types of curves, wing complexes can better adapt to irregular local curvature variations, thereby capturing more accurate topological features.

The rest of the paper is organized as follows. In Section 2, we provide a brief review of the definitions of the Čech complex, the Vietoris–Rips complex, and the ellipsoid complex. In Section 3, we present the definition of wing complexes and establish related theorems. In Section 4, we analyze and provide a detailed discussion of the topological properties of wing complexes. The proofs of the main results will be given in Section 5.

2. Persistent homology

Persistent homology is a method in topological data analysis for computing the topological features of data at different scales. In this section, we provide a brief overview of the fundamental concepts in persistent homology.

2.1. Simplicial complexes

Definition 1. *([25]) An **abstract simplicial complex** K is a finite collection of nonempty finite sets (called simplexes) which satisfies the subset-closure property: if a simplex $\sigma \in K$, then all of its*

subsets (called subsimplexes) also belong to K.

A filtered simplicial complex $K = \{K_\varepsilon\}$ is a collection of simplicial complexes for $0 \leq \varepsilon \in \mathbb{R}$ such that $K_\varepsilon \subset K_{\varepsilon'}$ if $\varepsilon \leq \varepsilon'$. Applying the homology functor to a filtered simplicial complex, we can get persistence modules, which can be decomposed as the direct sums of interval modules, by using the decomposition theorem in representation theory (see [14, 26]).

2.1.1. Čech and Vietoris–Rips complexes

Čech complexes and Vietoris–Rips complexes are two of the most widely used simplicial complexes in topological data analysis [16, 17]. For any $x \in \mathbb{R}^n$, denote by $B_\varepsilon(x) = \{x' \in \mathbb{R}^n \,|\, \|x - x'\| \leq \varepsilon\}$ the closed ball of radius ε centered at x.

Definition 2. *Given a finite set of points $X \subset \mathbb{R}^n$, σ is a set of points in X forming a simplex; the **Čech complex of** X **at scale** ε is the simplicial complex*

$$\check{C}_\varepsilon(X) = \{\sigma \subset X \,|\, \bigcap_{x\in\sigma} B_\varepsilon(x) \neq \emptyset\}. \tag{2.1}$$

Remark 1. *It is important to note that the union of the balls $\{B_\varepsilon(x)\}_{x\in X}$ forms an open cover of the topological space represented by the Čech complex $\check{C}_\varepsilon(X)$.*

Definition 3. *Given a finite set of points $X \subset \mathbb{R}^n$, the **Vietoris–Rips complex of** X **at scale** ε is the simplicial complex*

$$\mathrm{VR}_\varepsilon(X) = \{\sigma \subset X \,|\, d(x, y) \leq 2\epsilon \text{ for any } x, y \in \sigma\}, \tag{2.2}$$

where $d(\cdot, \cdot)$ is the Euclidean distance.

It is worth noting that the Čech complex is based on the common intersection of balls centered at data points, while the Vietoris–Rips complex relies on pairwise distances between points. On one hand, the Čech complex provides a more accurate representation of the underlying topology, because it is homotopy equivalent to the union of balls grown around the points with radius ε according to the Nerve Theorem [27]. On the other hand, under mild conditions in Euclidean space, it can be proved that

$$\check{C}_\varepsilon(X) \subseteq \mathrm{VR}_\varepsilon(X) \subseteq \check{C}_{\sqrt{2}\varepsilon}(X), \tag{2.3}$$

which means that the Vietoris–Rips complex serves as a computational approximation to the Čech complex [26]. In practical computations, the Vietoris–Rips complex is often preferred, particularly in high dimensions, due to its lower computational complexity.

Figure 1 shows an increasing sequence of Vietoris–Rips complexes in the plane [2]. We can observe that at time 0, there are four 0-dimensional simplices (vertices) a, b, c, and d. As the parameter ε increases, 1-dimensional simplices ab, bc, cd, and ad (edges) as well as 2-dimensional simplices abc and acd (triangles) are successively formed. Ultimately, at time 7, a 2-dimensional simplicial complex composed of two 2-dimensional simplices is formed. Throughout the process, each time step corresponds to a simplicial complex constructed at a given scale parameter ε, and each complex encodes a set of topological features. For instance, during time 0 to time 1, due to the enclosing ε-balls centered at a and b first intersect, the connected component a, b that existed at time 0 merges at time 1. This indicates that a 0-dimensional topological feature dies. Similarly, the connected component c

merges with ab at time 2, and d merges with the connected components ab and bc at time 3. It is noteworthy that at time 4, due to the connection between points a and d, a one-dimensional hole is born. At time 5, due to the connection between points a and c, a new connected component abc is formed. Finally, at time 6, due to the connection between points b and c, the one-dimensional hole that was born at time 4 disappears (gets filled).

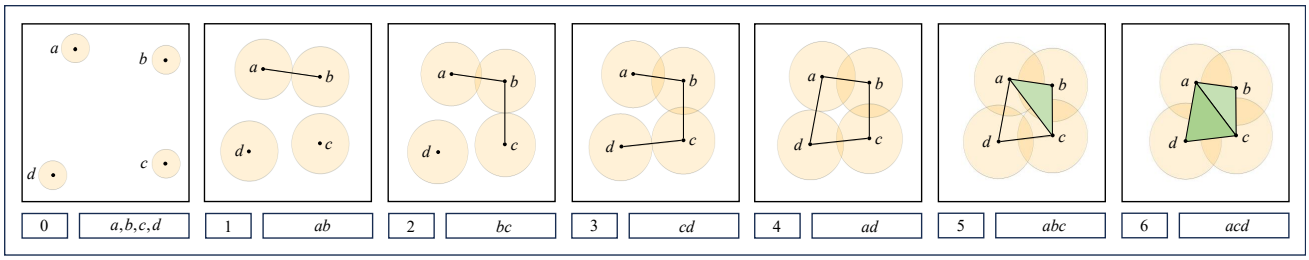

Figure 1. A filtered simplicial complex with newly added simplices.

The birth and death of these topological features mentioned above are recorded in the persistence diagram shown in Figure 2, where the horizontal coordinate represents the birth of the corresponding topological feature, and the vertical coordinate represents its death. As a result, all points in the persistence diagram lie above the diagonal $y = x$. It is important to note that points near the diagonal represent features that appear and disappear quickly and are usually regarded as noise. In contrast, points far from the diagonal are considered to be more persistent and are often interpreted as more meaningful topological features in point clouds.

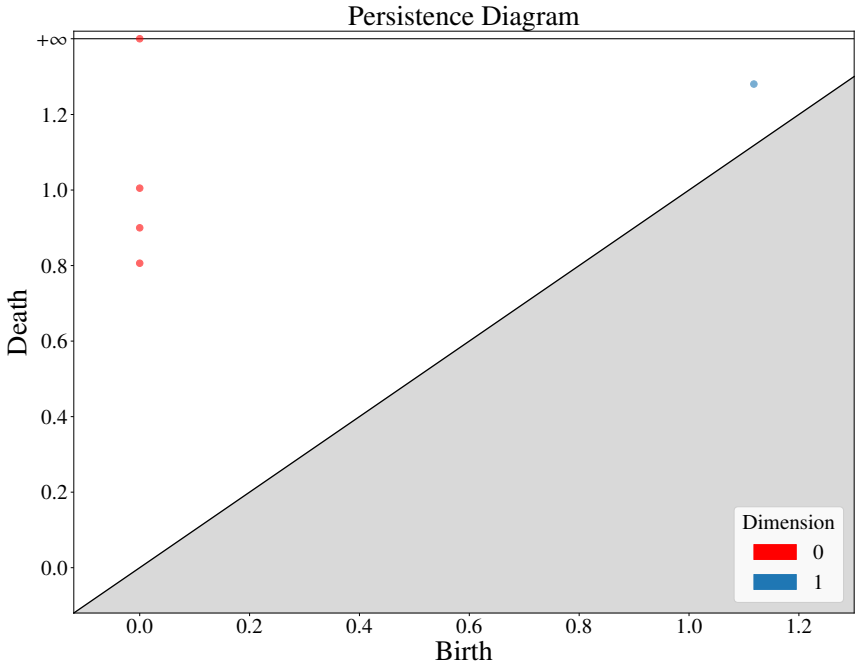

Figure 2. The persistence diagram corresponding to the filtered simplicial complex in Figure 1. The red points represent the birth and death of connected components (dimension 0), while the blue point represents the birth and death of a hole (dimension 1).

2.1.2. Ellipsoid complexes

Let $\mathcal{M}$ be a C^1-submanifold of $\mathbb{R}^n$; the **tangent-normal q-ellipsoid at scale ε at a point** $x \in \mathcal{M}$ is the closed ellipsoid $E^q_\varepsilon(x)$ in $\mathbb{R}^n$ with the center in x, the tangent semi-axes of length ε, and normal semi-axes of length ε/q. Assume that at point $x \in \mathcal{M}$, there is a tangent-normal coordinate system where the tangent semi-axes are aligned with the tangent space, and the normal semi-axes are aligned with the normal space. Let m denote the dimension of $\mathcal{M}$ at x; the **tangent-normal q-ellipsoids at scale ε at point** $x \in \mathcal{M}$ are given by ([24]):

$$E^q_\varepsilon(x) := \left\{ (x_1, \ldots, x_n) \in \mathbb{R}^n \;\middle|\; \frac{x_1^2 + \cdots + x_m^2}{\varepsilon^2} + \frac{x_{m+1}^2 + \cdots + x_n^2}{(\varepsilon/q)^2} \leq 1 \right\}. \tag{2.4}$$

Definition 4. *([24]) Let $\mathcal{M}$ be a C^1-submanifold of $\mathbb{R}^n$ and X a finite subset of $\mathcal{M}$. The **q-ellipsoid complex of X at scale** ε is the simplicial complex*

$$E^q_\varepsilon(X) = \{\sigma \subset X \,|\, E^q_\varepsilon(x) \cap E^q_\varepsilon(y) \neq \emptyset \text{ for any } x, y \in \sigma\}. \tag{2.5}$$

Remark 2. *Note that when $q = 1$, the ellipsoid $E^q_\varepsilon(x)$ becomes a Euclidean ball centered at x with radius ε. Therefore, the Čech complex can be regarded as a special case of the ellipsoid complex. Furthermore, although Definitions 3 and 4 share a similar structure, they differ conceptually. The Vietoris–Rips complex is defined based on pairwise distances between points, whereas the ellipsoid complex is constructed by considering when the enclosing ellipsoids of the points intersect.*

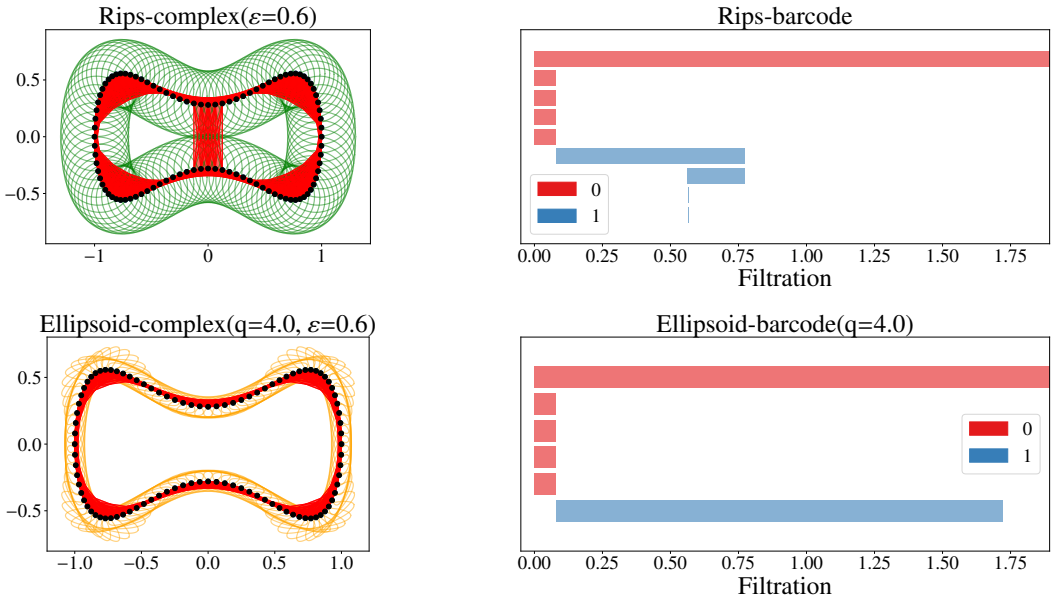

Figure 3. Comparison of the Rips complex and the ellipsoid complex on points sampled from a smooth curve. Top left: Rips complex at $\varepsilon = 0.6$. Bottom left: The ellipsoid complex for $q = 4$ at scale $\varepsilon = 0.6$. Top right: Rips-barcode. Bottom Right: Ellipsoid-barcode.

As shown in Figure 3, we consider a set of points sampled from a smooth curve resembling a dog bone [24]. From the left part of the figure, we observe that near the central part of the shape, the use of Rips complexes may lead to the enclosing balls intersecting too early, which results in the capture

of incorrect topological features. In contrast, ellipsoids offer anisotropic flexibility: their tangent axes can be stretched or contracted along tangent directions, and their normal axes can be adjusted along normal directions. Therefore, by tuning the shape parameters, ellipsoid complexes can adapt to rapid local geometric variations, thereby avoiding the premature formation of complexes and providing a more accurate approximation of the underlying structure.

The right half of Figure 3 shows the persistence barcodes corresponding to the two complexes; red intervals represent the persistence of connected components during the evolution of the simplicial complexes, and the blue intervals correspond to the persistence of one-dimensional holes. Notably, the barcode for the Rips complex contains two long blue intervals, indicating two persistence holes. However, for this shape, we would prefer to capture a single persistent hole rather than two. Therefore, using the ellipsoid complex is a better choice.

3. Wing complexes

In this section, we will introduce the wing complex for a finite set of points from a smooth plane curve.

3.1. Wing complexes

Let C be a smooth curve in $\mathbb{R}^2$ and $X \subset C$ a finite set of points such that the curvature in $x \in X$ is nonzero. For any $x \in X$, let

$$\alpha_x = -\frac{\overrightarrow{xO}}{|\overrightarrow{xO}|} \tag{3.1}$$

be the normal vector in x, where O is the center of curvature for x (see Figure 4).

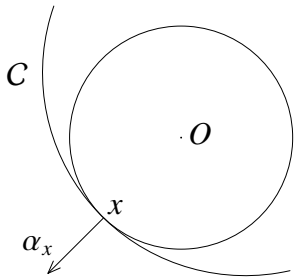

Figure 4. The normal vector α_x at a point $x \in C$.

Fix real numbers $0 \le \varepsilon$, $0 \le q \le 1$, and $0 \le \theta \le \pi/2$. For any $x \in X$, the **q, θ-wing at scale ε at the point** x (see Figure 5) is defined as

$$W_\varepsilon^{q,\theta}(x) = P(A, B, C, D) \cup P(A, B', C', D), \tag{3.2}$$

where

1) $\overrightarrow{xA} = q\varepsilon\alpha_x$ and $\overrightarrow{xD} = -q\varepsilon\alpha_x$,
2) $P(A, B, C, D)$ is the parallelogram with vertices A, B, C, D such that

$$\|\overrightarrow{AB}\| = \|\overrightarrow{CD}\| = \varepsilon, \tag{3.3}$$

and the angle between $\overrightarrow{AB}$ and $\overrightarrow{AD}$ is θ,

3) $P(A, B', C', D)$ is the parallelogram with vertices A, B', C', D such that

$$\|\overrightarrow{AB'}\| = \|\overrightarrow{C'D}\| = \varepsilon, \tag{3.4}$$

and the angle between $\overrightarrow{AB'}$ and $\overrightarrow{AD}$ is θ.

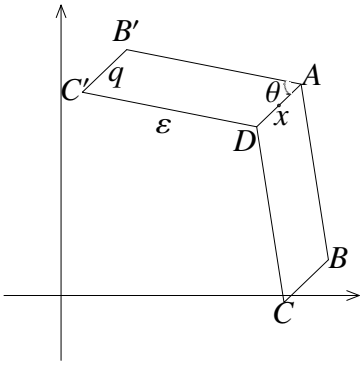

Figure 5. The q, θ-wing at scale ε at point x.

Definition 5. *Let C be a smooth curve in $\mathbb{R}^2$ and $X \subset C$ a finite set of points such that the curvature in $x \in X$ is nonzero. The q, θ-**wing complex of** X **at scale** ε is defined as*

$$W_\varepsilon^{q,\theta}(X) = \{\sigma \subset X \mid W_\varepsilon^{q,\theta}(x) \cap W_\varepsilon^{q,\theta}(y) \neq \emptyset \text{ for any } x, y \in \sigma\}. \tag{3.5}$$

Note that $E_\varepsilon^{1/q}(x) \subset W_\varepsilon^{q,\pi/2}(x) \subset E_{\varepsilon'}^{1/q}(x)$, where $\varepsilon' = \sqrt{2}\varepsilon$. Hence, we have

$$E_\varepsilon^{1/q}(X) \subset W_\varepsilon^{q,\pi/2}(X) \subset E_{\varepsilon'}^{1/q}(X), \tag{3.6}$$

if $q = 0$, we also have $E_\varepsilon^\infty(x) = W_\varepsilon^{0,\pi/2}(x)$ and $E_\varepsilon^\infty(X) = W_\varepsilon^{0,\pi/2}(X)$.

To more intuitively illustrate the wing complex and its advantages over the Rips complex on some special curves, we use the framework for computing persistent homology proposed by Kališnik et al. [24], within which we incorporate the algorithm for computing persistent homology via the wing complex. As shown in Figure 6, consider a point cloud obtained by exact sampling from a smooth curve resembling a dog bone, where the exact normal vector of each sampled point can be derived from the second derivative of the original function. Figure 6 illustrates wing complexes at different scales ($\varepsilon = 0.1, 0.2, 0.3, 0.4$) when $\varepsilon/q = 3$ and the angle between the parallelogram wings and the symmetry axis $\theta = \pi/4$.

When constructing wing complexes, the orientation of each wing is determined by the normal vectors of the sampled points. For the type of data illustrated in Figure 6, in the bottleneck region where the normals point inward, increasing ε drives the wings to extend outward, thereby preventing premature intersections of the complexes associated with points in this region. As shown in Figure 7, the wing-barcode exhibits a single long bar in the 1-dimensional homology, whereas the Rips-barcode incorrectly reveals two features. This result demonstrates that the wing complex can more accurately capture the fundamental topological structure of some special curves.

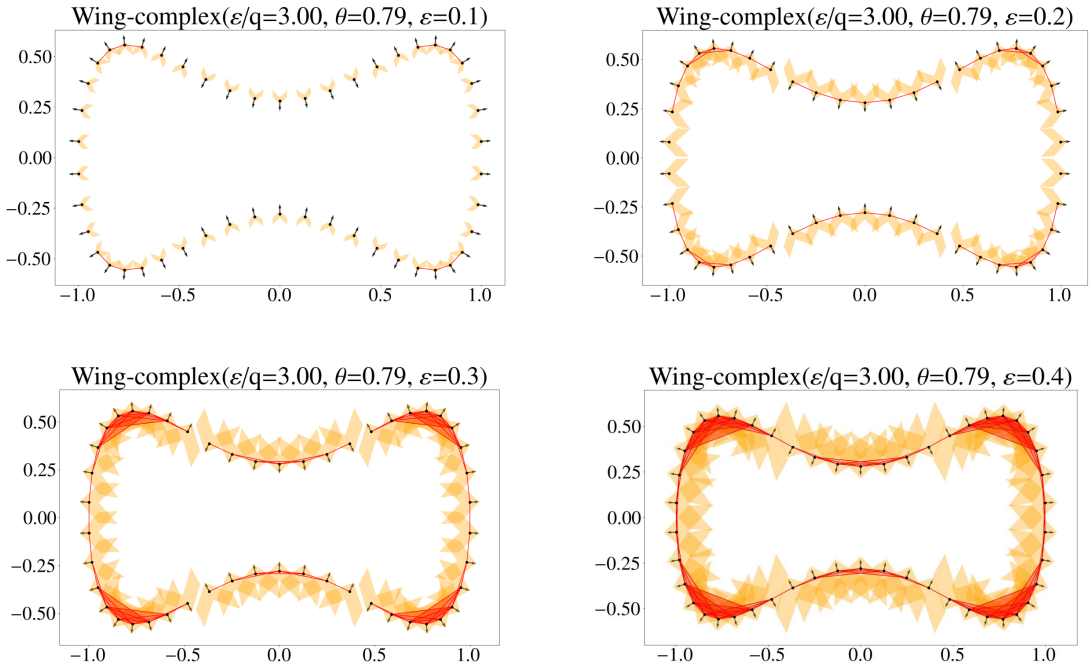

Figure 6. Wing complexes for $\varepsilon/q = 3$ and $\theta = \pi/4$ at scales $\varepsilon = 0.1$, $\varepsilon = 0.2$, $\varepsilon = 0.3$ and $\varepsilon = 0.4$ for a point cloud sampled from a smooth curve resembling a dog bone.

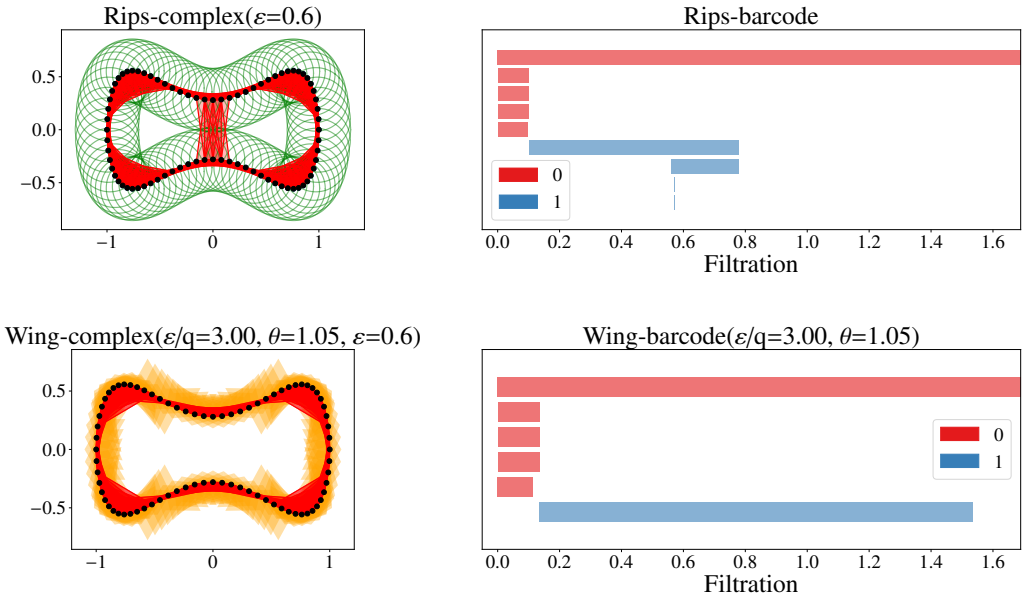

Figure 7. Top left: The Rips complex at scale $\varepsilon = 0.6$. Bottom left: The wing complex for $\varepsilon/q = 3$ and $\theta = \pi/3$ at scale $\varepsilon = 0.6$. Top right: Rips-barcode. Bottom Right: Wing-barcode.

3.2. *Properties*

In this section, the relations between $W_\varepsilon^{0,\theta}(X)$ and $W_\varepsilon^{0,\pi/2}(X)$ will be studied.
For any two points $x, y \in X$, denote by $\varepsilon_{q,\theta}(x, y)$ the minimal ε such that

$$W_\varepsilon^{q,\alpha}(x) \cap W_\varepsilon^{q,\alpha}(y) \neq \emptyset. \tag{3.7}$$

Hence, we have

$$W_{\varepsilon}^{q,\theta}(X) = \{\sigma \subset X \,|\, \varepsilon_{q,\theta}(x,y) \leq \varepsilon \text{ for any } x,y \in \sigma\}. \tag{3.8}$$

Let L_x (resp. L_y) be the tangent in x (resp. y). Denote by z the intersection of L_x and L_y. Let l_x (resp. l_y) be the distance between x (resp. y) and z. Note that

$$\varepsilon_{0,\pi/2}(x,y) = \max\{l_x, l_y\}. \tag{3.9}$$

Let $L_x(\theta)$ (resp. $L_y(\theta)$) be the rays with endpoint x (resp. y) such that the angle between $L_x(\theta)$ (resp. $L_y(\theta)$) and α_x (resp. α_y) is $\pi - \theta$. Denote by $z(\theta)$ the intersection of $L_x(\theta)$ and $L_y(\theta)$. Let $l_x(\theta)$ (resp. $l_y(\theta)$) be the distance between x (resp. y) and $z(\theta)$. Note that

$$\varepsilon_{0,\theta}(x,y) = \max\{l_x(\theta), l_y(\theta)\}. \tag{3.10}$$

Let $\varphi_{x,y}$ be the angle from α_x to $\overrightarrow{xy}$ along α_y and $\alpha_{x,y}$ the angle between α_x and α_y.

Theorem 1. *For any two points x and y in X, we have*

$$\varepsilon_{0,\theta}(x,y) < \varepsilon_{0,\pi/2}(x,y) \tag{3.11}$$

if one of the following conditions is satisfied:

1) $\alpha_{x,y} < \pi/2$, $\varphi_{x,y} \in (\alpha_{x,y}/2, \alpha_{x,y})$, $\theta \in (0, \varphi_{x,y} - \alpha_{x,y}/2)$,
2) $\alpha_{x,y} < \pi/2$, $\varphi_{x,y} \in (\pi/2, \pi/2 + \alpha_{x,y})$, $\theta \in (0, \alpha_{x,y})$,
3) $\alpha_{x,y} < \pi/2$, $\varphi_{x,y} \in (\pi, \pi + \alpha_{x,y}/2)$, $\theta \in (0, \pi + \alpha_{x,y}/2 - \varphi_{x,y})$,
4) $\alpha_{x,y} < \pi/2$, $\varphi_{x,y} \in (\pi + \alpha_{x,y}, 3\pi/2)$, $\theta \in (0, 3\pi/2 - \varphi_{x,y})$,
5) $\alpha_{x,y} < \pi/2$, $\varphi_{x,y} \in (3\pi/2 + \alpha_{x,y}, 2\pi)$, $\theta \in (0, \varphi_{x,y} - 3\pi/2 - \alpha_{x,y})$,
6) $\alpha_{x,y} > \pi/2$, $\varphi_{x,y} \in (\alpha_{x,y}/2, \pi/2)$, $\theta \in (0, \varphi_{x,y} - \alpha_{x,y}/2)$,
7) $\alpha_{x,y} > \pi/2$, $\varphi_{x,y} \in (\pi/2, \pi/2 + \alpha_{x,y})$, $\theta \in (0, \alpha_{x,y})$,
8) $\alpha_{x,y} > \pi/2$, $\varphi_{x,y} \in (\pi/2 + \alpha_{x,y}, \pi + \alpha_{x,y}/2)$, $\theta \in (0, \pi + \alpha_{x,y}/2 - \varphi_{x,y})$.

Theorem 2. *For any two points x and y in X, we have*

$$\varepsilon_{0,\theta}(x,y) > \varepsilon_{0,\pi/2}(x,y) \tag{3.12}$$

if one of the following conditions is satisfied:

1) $\alpha_{x,y} < \pi/2$, $\varphi_{x,y} \in (0, \alpha_{x,y}/2)$, $\theta \in (0, \varphi_{x,y})$,
2) $\alpha_{x,y} < \pi/2$, $\varphi_{x,y} \in (\alpha_{x,y}, \pi/2)$, $\theta \in (0, \varphi_{x,y} - \alpha_{x,y})$,
3) $\alpha_{x,y} < \pi/2$, $\varphi_{x,y} \in (\pi/2 + \alpha_{x,y}, \pi)$, $\theta \in (0, \pi - \varphi_{x,y})$,
4) $\alpha_{x,y} < \pi/2$, $\varphi_{x,y} \in (\pi + \alpha_{x,y}/2, \pi + \alpha_{x,y})$, $\theta \in (0, \pi + \alpha_{x,y} - \varphi_{x,y})$,
5) $\alpha_{x,y} < \pi/2$, $\varphi_{x,y} \in (3\pi/2, 3\pi/2 + \alpha_{x,y})$, $\theta_{x,y} \in (0, \pi/2 - \alpha_{x,y}/2)$,
6) $\alpha_{x,y} > \pi/2$, $\varphi_{x,y} \in (\alpha_{x,y} - \pi/2, \alpha_{x,y}/2)$, $\theta \in (0, \pi/2 + \varphi_{x,y} - \alpha_{x,y})$,
7) $\alpha_{x,y} > \pi/2$, $\varphi_{x,y} \in (\pi + \alpha_{x,y}/2, 3\pi/2)$, $\theta \in (0, 3\pi/2 - \varphi_{x,y})$,
8) $\alpha_{x,y} > \pi/2$, $\varphi_{x,y} \in (3\pi/2, 3\pi/2 + \alpha_{x,y})$, $\theta \in (0, \pi/2 - \alpha_{x,y}/2)$.

Remark 3. *Assume that $\alpha_{x,y} < \pi/2$.*

If the angle from α_x to $\overrightarrow{xz}$ is $\pi/2$, let A_0, A_1, A_2 be three points in L_y such that $\overrightarrow{xA_0}$ is orthogonal to L_x, $|\overrightarrow{zx}| = |\overrightarrow{zA_1}|$, and $\overrightarrow{xA_2}$ is orthogonal to L_y (see Figure 8). In this case, we denote z by z_1.

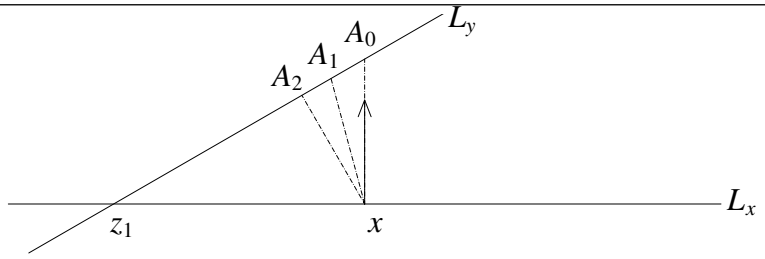

Figure 8. The case where $\alpha_{x,y} < \pi/2$, and the angle from α_x to $\vec{xz}$ is $\pi/2$.

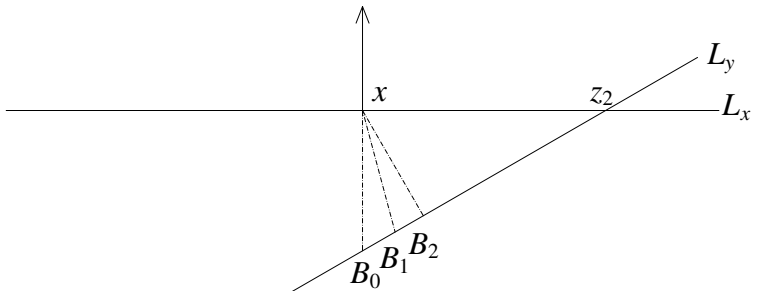

Figure 9. The case where $\alpha_{x,y} < \pi/2$, and the angle from α_x to $\vec{xz}$ is $3\pi/2$.

If the angle from α_x to $\vec{xz}$ is $3\pi/2$, let B_0, B_1, B_2 be three points in L_y such that $\overrightarrow{xB_0}$ is orthogonal to L_x, $|\vec{zx}| = |\overrightarrow{zB_1}|$, and $\overrightarrow{xB_2}$ is orthogonal to L_y (see Figure 9). In this case, we denote z by z_2.

Then, we have the following correspondences:

1) $\varphi_{x,y} \in (0, \alpha_{x,y}/2)$ *if and only if y is between A_0 and A_1,*
2) $\varphi_{x,y} \in (\alpha_{x,y}/2, \alpha_{x,y})$ *if and only if y is between A_1 and A_2,*
3) $\varphi_{x,y} \in (\alpha_{x,y}, \pi/2)$ *if and only if y is between A_2 and z_1,*
4) $\varphi_{x,y} \in (\pi/2, \pi/2 + \alpha_{x,y})$ *if and only if y is in the outside of z_1,*
5) $\varphi_{x,y} \in (\pi/2 + \alpha_{x,y}, \pi)$, *if and only if y is in the outside of B_0,*
6) $\varphi_{x,y} \in (\pi, \pi + \alpha_{x,y}/2)$ *if and only if y is between B_0 and B_1,*
7) $\varphi_{x,y} \in (\pi + \alpha_{x,y}/2, \pi + \alpha_{x,y})$ *if and only if y is between B_1 and B_2,*
8) $\varphi_{x,y} \in (\pi + \alpha_{x,y}, 3\pi/2)$ *if and only if y is between B_2 and z_2,*
9) $\varphi_{x,y} \in (3\pi/2, 3\pi/2 + \alpha_{x,y})$ *if and only if y is in the outside of z_2,*
10) $\varphi_{x,y} \in (3\pi/2 + \alpha_{x,y}, 2\pi)$ *if and only if y is in the outside of A_0.*

Remark 4. *Assume that $\alpha_{x,y} > \pi/2$.*

If the angle from α_x to $\vec{xz}$ is $\pi/2$, let C be a point in L_y such that $|\vec{zx}| = |\overrightarrow{zC}|$ (see Figure 10). In this case, we denote z by z_1.

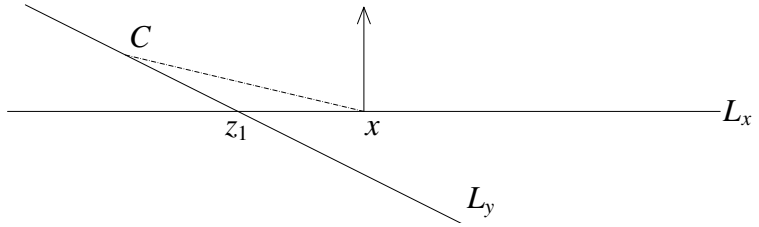

Figure 10. The case where $\alpha_{x,y} > \pi/2$, and the angle from α_x to $\vec{xz}$ is $\pi/2$.

If the angle from α_x to $\overrightarrow{xz}$ is $3\pi/2$, let D be a point in L_y such that $|\overrightarrow{zx}| = |\overrightarrow{zD}|$ (see Figure 11). In this case, we denote z by z_2.

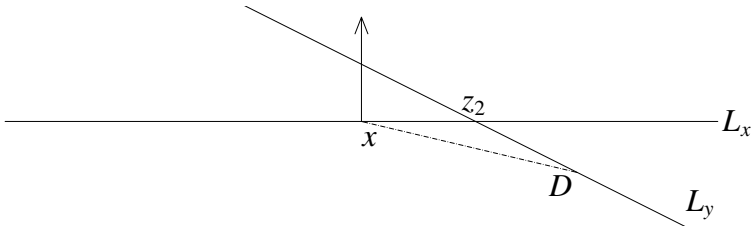

Figure 11. The case where $\alpha_{x,y} > \pi/2$, and the angle from α_x to $\vec{xz}$ is $3\pi/2$.

Then, we have the following correspondences:

1) $\varphi_{x,y} \in (\alpha_{x,y} - \pi/2, \alpha_{x,y}/2)$ *if and only if y is in the outside of C,*
2) $\varphi_{x,y} \in (\alpha_{x,y}/2, \pi/2)$ *if and only if y is between C and z_1,*
3) $\varphi_{x,y} \in (\pi/2, \alpha_{x,y} + \pi/2)$ *if and only if y is in the outside of z_1,*
4) $\varphi_{x,y} \in (\alpha_{x,y} + \pi/2, \alpha_{x,y}/2 + \pi)$ *if and only if y is in the outside of D,*
5) $\varphi_{x,y} \in (\alpha_{x,y}/2 + \pi, 3\pi/2)$ *if and only if y is between D and z_2,*
6) $\varphi_{x,y} \in (3\pi/2, \alpha_{x,y} + 3\pi/2)$ *if and only if y is in the outside of z_2.*

4. Topological properties of Wing complexes

In this section, we investigate the relationship between the wing complex and angular parameters for certain types of special curves based on the theorems established earlier. As applications of Theorems 1 and 2, we have the following propositions for some special curves.

Proposition 1. *Let C be a smooth curve such that it is the boundary of a convex domain in $\mathbb{R}^2$ and $X \subset C$ a finite set of points such that the curvature in $x \in X$ is nonzero. Then,*

$$W_\varepsilon^{0,\pi/2}(X) \subset W_\varepsilon^{0,\theta}(X) \tag{4.1}$$

for $0 < \theta < \pi/2$ such that $\pi/2 - \theta$ is small enough.

Proof. For any points x and y in X, they satisfy condition (2) or condition (7) in Theorem 1. Hence,

$$\varepsilon_{0,\theta}(x, y) < \varepsilon_{0,\pi/2}(x, y), \tag{4.2}$$

and we get the desired result. □

Although we have only discussed the properties of wing complexes when $q = 0$, through practical computations of persistent homology for the case where $q \neq 0$, we found that these properties still hold. Example 1 provides an intuitive explanation of the intersection between two wing complexes when $q \neq 0$.

Example 1. *Let X be a finite set from a circle with radius r and center O and x, y be two points in X such that the angle between $\overrightarrow{Ox}$ and $\overrightarrow{Oy}$ is φ (see Figure 12). Then, we have*

$$\varepsilon_{q,\theta}(x, y) = \frac{r \sin \varphi/2}{q \sin \varphi/2 + \sin(\alpha + \varphi/2)}. \tag{4.3}$$

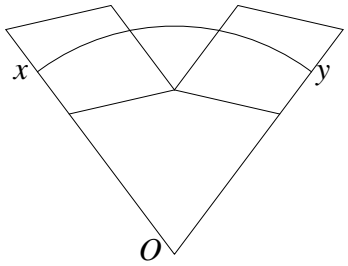

Figure 12. The intersection of wing complexes corresponding to two points x and y sampled from a circle. The left parallelogram represents the right half wing complex of point x, and the right parallelogram represents the left half wing complex of point y.

Remark 5. *Proposition 1 implies that the birth of each new topological feature in $W_\varepsilon^{0,\theta}(X)$ is earlier than that in $W_\varepsilon^{0,\pi/2}(X)$. For example, when the curve is a circle, as shown in Figure 13, the left endpoint of the blue bar records the birth time of the* 1*-dimensional topological feature. It can be observed that when $\pi/2-\theta$ is small enough, the birth time of the* 1*-dimensional feature corresponding to $\theta = 19\pi/40$ is earlier than that for $\theta = \pi/2$.*

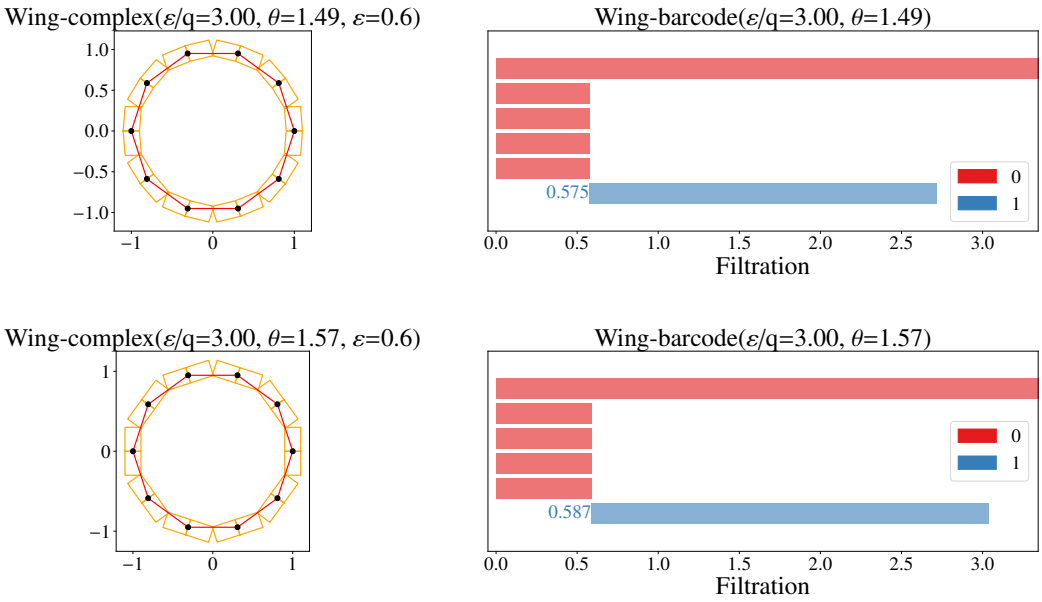

Figure 13. Top: The wing complex for $\varepsilon/q = 3$ and $\theta = 19\pi/40$ at scale $\varepsilon = 0.6$ for a point cloud sampled from a circle. Bottom: The wing complex for $\varepsilon/q = 3$ and $\theta = \pi/2$ at scale $\varepsilon = 0.6$ for a point cloud sampled from a circle.

Proposition 2. *Let C be a curve consisting of arcs and $X \subset C$ a finite set of points such that the curvature in $x \in X$ is nonzero. For any two points x and y in X such that they are in the same arc or in neighboring arcs, and the degrees from x and y to the intersection are both less than $\pi/4$, we have*

$$\varepsilon_{0,\theta}(x, y) < \varepsilon_{0,\pi/2}(x, y). \tag{4.4}$$

Proof. The points x and y satisfy condition (7) or condition (8) in Theorem 1. Hence,

$$\varepsilon_{0,\theta}(x, y) < \varepsilon_{0,\pi/2}(x, y), \tag{4.5}$$

and we get the desired result. □

Remark 6. *Proposition 2 implies that the birth of the connectness in $W_\varepsilon^{0,\theta}(X)$ is earlier than that in $W_\varepsilon^{0,\pi/2}(X)$.*

Proposition 3. *Let C_1 and C_2 be two arcs such that they are on different sides of the tangent of each $x \in C_1 \cup C_2$. For points $x \in C_1$ and $y \in C_2$, we have*

$$\varepsilon_{0,\theta}(x, y) > \varepsilon_{0,\pi/2}(x, y). \tag{4.6}$$

Proof. For points $x \in C_1$ and $y \in C_2$, they satisfy condition (5) or condition (8) in Theorem 2. Hence,

$$\varepsilon_{0,\theta}(x, y) > \varepsilon_{0,\pi/2}(x, y), \tag{4.7}$$

and we get the desired result. □

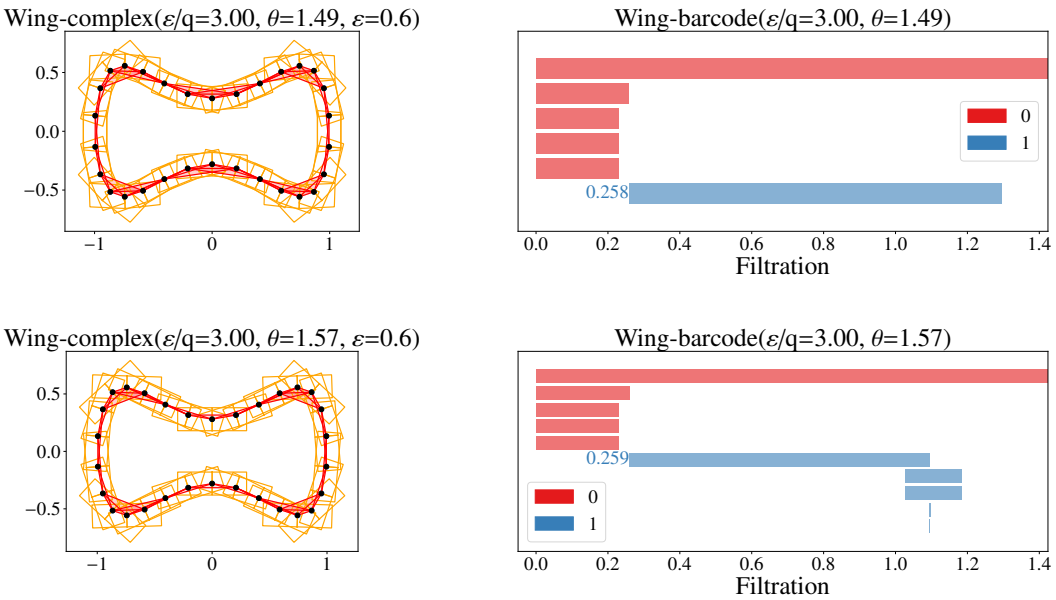

Figure 14. Top: The wing complex for $\varepsilon/q = 3$ and $\theta = 19\pi/40$ at scale $\varepsilon = 0.6$ for a point cloud sampled from a smooth curve resembling a dog bone. Bottom: The wing complex for $\varepsilon/q = 3$ and $\theta = \pi/2$ at scale $\varepsilon = 0.6$ for a point cloud sampled from a smooth curve resembling a dog bone.

Remark 7. *For two sets X_1 and X_2 of points, define*

$$\varepsilon_{0,\theta}(X_1, X_2) = \min\{\varepsilon_{0,\theta}(x_1, x_2) \,|\, x_1 \in X_1, x_2 \in X_2\}. \tag{4.8}$$

Then Proposition 3 implies that

$$\varepsilon_{0,\theta}(C_1, C_2) > \varepsilon_{0,\pi/2}(C_1, C_2), \tag{4.9}$$

and the moment that two connected components meet in $W_\varepsilon^{0,\theta}(X)$ is later than that in $W_\varepsilon^{0,\pi/2}(X)$.

Propositions 2 and 3 can be illustrated using the same example (see Figure 14). For a smooth curve resembling a dog bone, it can be observed that the curve has four inflection points where the

curvature changes significantly. The arcs connected at the left and right sides of each inflection point can be regarded as the curve C defined in Proposition 2, while the two inwardly convex arcs at the top and bottom can be regarded as the curves C_1 and C_2 defined in Proposition 3. When the curve is exactly sampled, the inflection points are excluded, and the precise normal vectors of the sampled points are obtained from the second derivative of the original function, all of which are nonzero. From the persistence barcodes shown on the right side of Figure 14, it can be observed that the birth time of the 1-dimensional topological feature corresponding to $\theta = 19\pi/40$ is earlier, and its death time is later than that for $\theta = \pi/2$. This indicates that the 1-dimensional topological feature corresponding to $\theta = 19\pi/40$ is more persistent.

Remark 8. *If X is an accurate sample in C, then it is reasonable to let $q = 0$. But it is not reasonable if X is not an accurate sample.*

In addition to the experiments mentioned earlier, we also designed a comparative experiment between the wing complex and the ellipsoid complex and discussed the computational cost of the wing complex. We compared the wing complex and the ellipsoid complex on the aforementioned dog-bone-shaped curve where the bottleneck region is narrower than before. As shown in Figure 15, in the persistence barcodes, the first 1-dimensional barcode in the wing complex is born earlier, and the second 1-dimensional barcode appears later than in the ellipsoid complex. This indicates that, for this type of curve, the wing complex captures the one-dimensional hole earlier than the ellipsoid complex while effectively preventing premature intersections across the narrow bottleneck region, thereby leading to a more accurate topological feature.

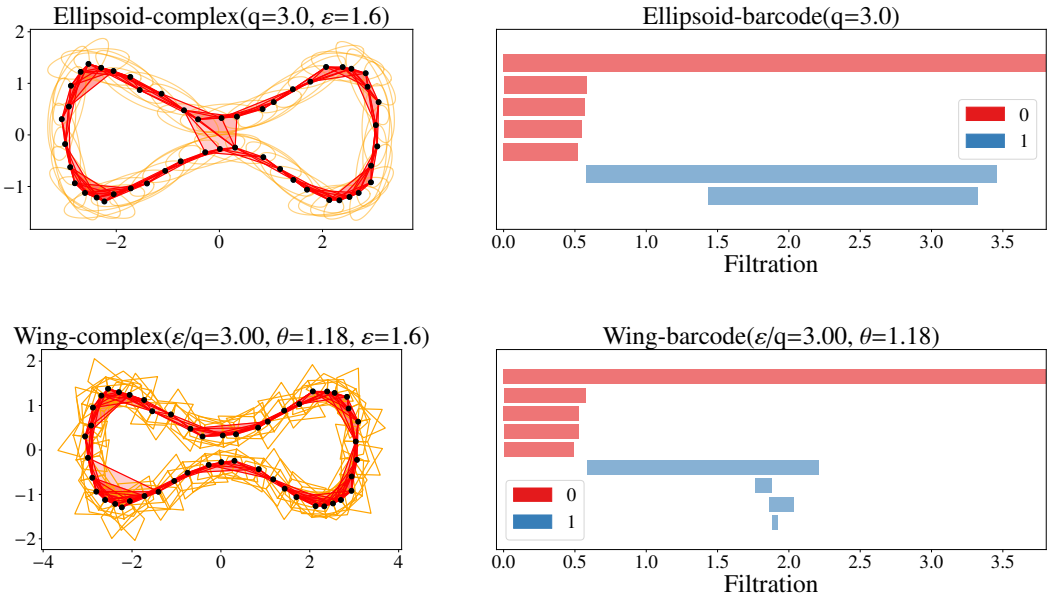

Figure 15. Top: The ellipsoid complex for $q = 3$ at scale $\varepsilon = 0.6$ for a point cloud sampled from a smooth plane curve with mild geometric perturbations. Bottom: The wing complex for $\varepsilon/q = 3$ and $\theta = 3\pi/8$ at scale $\varepsilon = 0.6$ for a point cloud sampled from a smooth plane curve with mild geometric perturbations.

To further validate the performance of the wing complex, in addition to the circle and dog-bone-shaped curves, we also conducted experiments on some irregular curves containing narrow bottleneck

regions. We found that, on these curves, the experimental results of the wing complex outperform those of the Rips complex in most cases. Moreover, it is important to note that when $\theta = \pi/2$, the wing complex forms a rectangle with length 2ε and width q, and its topological properties are similar to those of the ellipsoid complex. Therefore, under general conditions, by properly adjusting the parameter θ, the experimental results of the wing complex and the ellipsoid complex on these irregular curves exhibit a certain degree of similarity.

In terms of computational cost, we conducted tests on the curves discussed above. For the purpose of accurately comparing the computational costs of Rips complexes, ellipsoid complexes, and wing complexes, we integrated the wing complex into the code provided by Kališnik et al. for unified computation [24]. For each number of sample points n, we took the average of ten repeated computations and performed curve fitting for each complex type. As shown in Figure 16, the existing method for computing persistent homology based on the Rips complex is well established, which results in the fastest computation time. When the number of sample points is small, the computational costs of wing complexes and ellipsoid complexes are similar. However, as the data size increases, the computation time of wing complexes increases significantly. In addition, for different types of curves, the wing complex requires additional adjustment of the angular parameter θ to ensure accuracy, which incurs additional computational cost.

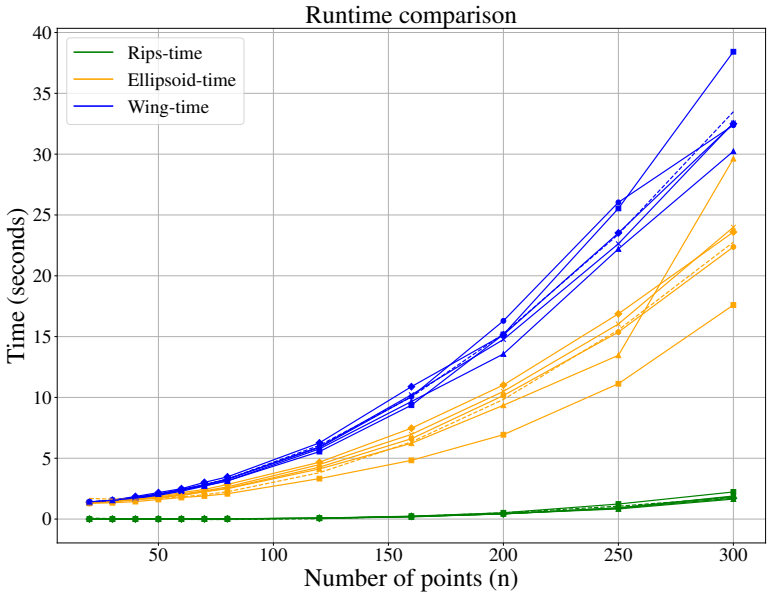

Figure 16. Comparison of computational runtime for Rips complexes, ellipsoid complexes, and wing complexes across varying numbers of sample points n.

In summary, based on the topological properties of the wing complex and the computational experiments, the wing complex is particularly well suited for smooth plane curves with narrow bottleneck regions. When dealing with such curves, the main advantage of the wing complex lies in its ability to extend outward in the bottleneck region where the normal vectors point inward by increasing the value of q, thus preventing the complexes associated with the points in that region from intersecting prematurely. Furthermore, considering both the experimental results and computational cost, we can conclude that the ellipsoid complex is more appropriate for curves that are precisely sampled, with

a large number of sample points and narrow bottleneck regions, whereas the wing complex is more suitable for curves with fewer sample points or curves with noise in the narrow bottleneck region.

5. Proofs of Theorems 1 and 2

In this section, we will check Theorems 1 and 2 together case by case.

Proof. To begin, assume that $\alpha_{x,y} < \pi/2$.

1) $\varphi_{x,y} \in (0, \alpha_{x,y}/2)$ (see Figure 17). Now, $l_x < l_y$. Because the center of $C_{x,y,z}$ (the circle that contains x, y, and z) is in the interior of the triangle Δxyz, we have

$$l_x(\theta) < l_x, l_y < l_y(\theta), l_x(\theta) < l_y(\theta), \tag{5.1}$$

when $\theta \in (0, \varphi_{x,y})$. Hence,

$$\varepsilon_{0,\theta}(x, y) = l_y(\theta) > l_y = \varepsilon_{0,\pi/2}(x, y). \tag{5.2}$$

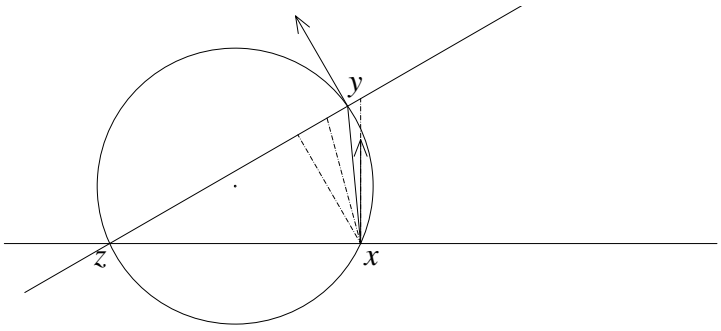

Figure 17. The case of $\alpha_{x,y} < \pi/2$ and $\varphi_{x,y} \in (0, \alpha_{x,y}/2)$.

2) $\varphi_{x,y} \in (\alpha_{x,y}/2, \alpha_{x,y})$ (see Figure 18). Now, $l_x > l_y$. Because the center of $C_{x,y,z}$ is in the interior of the triangle Δxyz, we have

$$l_y < l_y(\theta) < l_x(\theta) < l_x, \tag{5.3}$$

when $\theta \in (0, \varphi_{x,y} - \alpha_{x,y}/2)$. Hence,

$$\varepsilon_{0,\theta}(x, y) = l_x(\theta) < l_x = \varepsilon_{0,\pi/2}(x, y). \tag{5.4}$$

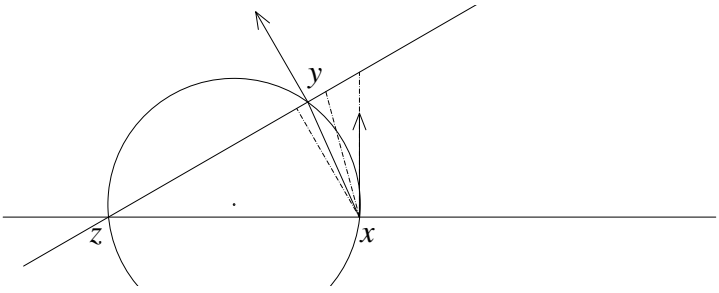

Figure 18. The case of $\alpha_{x,y} < \pi/2$ and $\varphi_{x,y} \in (\alpha_{x,y}/2, \alpha_{x,y})$.

3) $\varphi_{x,y} \in (\alpha_{x,y}, \pi/2)$ (see Figure 19). Now, $l_x > l_y$. Because the center of $C_{x,y,z}$ is in the exterior of the triangle Δxyz, we have

$$l_x < l_x(\theta), l_y < l_y(\theta), l_y(\theta) < l_x(\theta), \tag{5.5}$$

when $\theta \in (0, \varphi_{x,y} - \alpha_{x,y})$. Hence,

$$\varepsilon_{0,\theta}(x, y) = l_x(\theta) > l_x = \varepsilon_{0,\pi/2}(x, y). \tag{5.6}$$

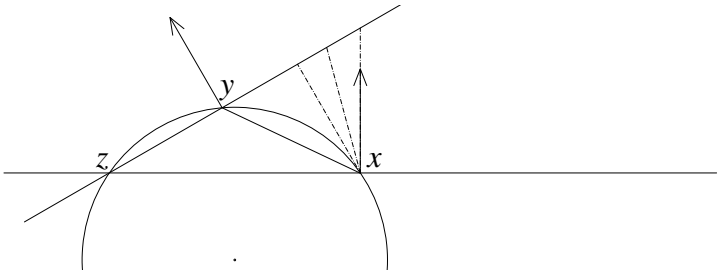

Figure 19. The case of $\alpha_{x,y} < \pi/2$ and $\varphi_{x,y} \in (\alpha_{x,y}, \pi/2)$.

4) $\varphi_{x,y} \in (\pi/2, \pi/2 + \alpha_{x,y})$ (see Figure 20). Now,

$$l_x(\theta) < \max\{l_x, l_y\}, l_y(\theta) < \max\{l_x, l_y\}, \tag{5.7}$$

when $\theta \in (0, \alpha_{x,y})$. Hence,

$$\varepsilon_{0,\theta}(x, y) = \max\{l_x(\theta), l_y(\theta)\} < \max\{l_x, l_y\} = \varepsilon_{0,\pi/2}(x, y). \tag{5.8}$$

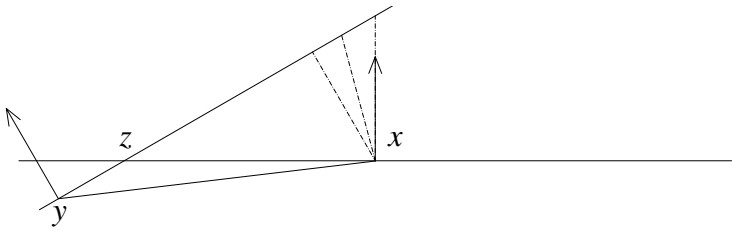

Figure 20. The case of $\alpha_{x,y} < \pi/2$ and $\varphi_{x,y} \in (\pi/2, \pi/2 + \alpha_{x,y})$.

5) $\varphi_{x,y} \in (\pi/2 + \alpha_{x,y}, \pi)$ (see Figure 21). Now, $l_x < l_y$. Because the center of $C_{x,y,z}$ is in the exterior of the triangle Δxyz, we have

$$l_x < l_x(\theta), l_y < l_y(\theta), l_x(\theta) < l_y(\theta), \tag{5.9}$$

when $\theta \in (0, \pi - \varphi_{x,y})$. Hence,

$$\varepsilon_{0,\theta}(x, y) = l_y(\theta) > l_y = \varepsilon_{0,\pi/2}(x, y). \tag{5.10}$$

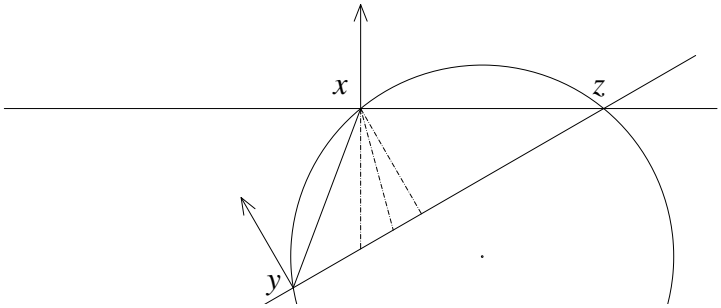

Figure 21. The case of $\alpha_{x,y} < \pi/2$ and $\varphi_{x,y} \in (\pi/2 + \alpha_{x,y}, \pi)$.

6) $\varphi_{x,y} \in (\pi, \pi + \alpha_{x,y}/2)$ (see Figure 22). Now, $l_x < l_y$. Because the center of $C_{x,y,z}$ is in the interior of the triangle Δxyz, we have

$$l_x < l_x(\theta) < l_y(\theta) < l_y, \tag{5.11}$$

when $\theta \in (0, \pi + \alpha_{x,y}/2 - \varphi_{x,y})$. Hence,

$$\varepsilon_{0,\theta}(x, y) = l_y(\theta) < l_y = \varepsilon_{0,\pi/2}(x, y). \tag{5.12}$$

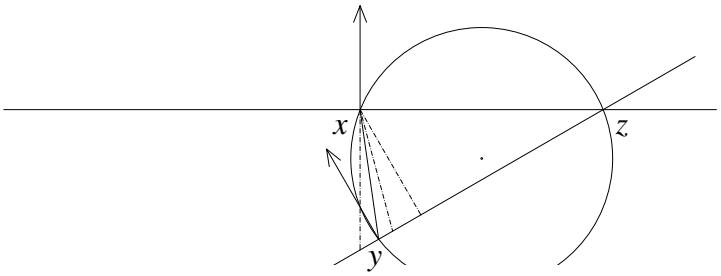

Figure 22. The case of $\alpha_{x,y} < \pi/2$ and $\varphi_{x,y} \in (\pi, \pi + \alpha_{x,y}/2)$.

7) $\varphi_{x,y} \in (\pi + \alpha_{x,y}/2, \pi + \alpha_{x,y})$ (see Figure 23). Now, $l_x > l_y$. Because the center of $C_{x,y,z}$ is in the interior of the triangle Δxyz, we have

$$l_x < l_x(\theta), l_y(\theta) < l_y, l_y(\theta) < l_x(\theta), \tag{5.13}$$

when $\theta \in (0, \pi + \alpha_{x,y} - \varphi_{x,y})$. Hence,

$$\varepsilon_{0,\theta}(x, y) = l_x(\theta) > l_x = \varepsilon_{0,\pi/2}(x, y). \tag{5.14}$$

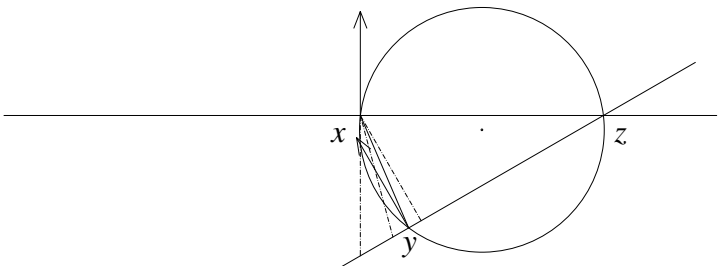

Figure 23. The case of $\alpha_{x,y} < \pi/2$ and $\varphi_{x,y} \in (\pi + \alpha_{x,y}/2, \pi + \alpha_{x,y})$.

8) $\varphi_{x,y} \in (\pi + \alpha_{x,y}, 3\pi/2)$ (see Figure 24). Now, $l_x > l_y$. Because the center of $C_{x,y,z}$ is in the exterior of the triangle Δxyz, we have

$$l_x(\theta) < l_x, l_y(\theta) < l_y, l_y(\theta) < l_x(\theta), \tag{5.15}$$

when $\theta \in (0, 3\pi/2 - \varphi_{x,y})$. Hence,

$$\varepsilon_{0,\theta}(x, y) = l_x(\theta) < l_x = \varepsilon_{0,\pi/2}(x, y). \tag{5.16}$$

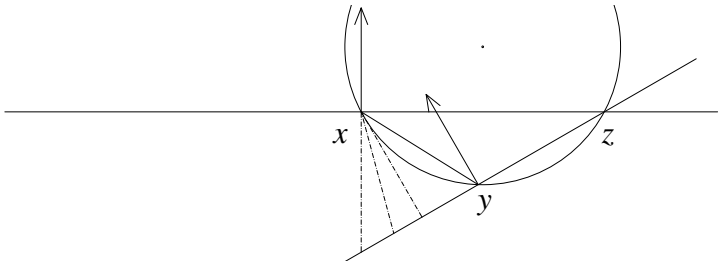

Figure 24. The case of $\alpha_{x,y} < \pi/2$ and $\varphi_{x,y} \in (\pi + \alpha_{x,y}, 3\pi/2)$.

9) $\varphi_{x,y} \in (3\pi/2, 3\pi/2 + \alpha_{x,y})$ (see Figure 25). Now,

$$l_x < l_x(\theta), l_y < l_y(\theta), \tag{5.17}$$

when $\theta \in (0, \pi/2 - \alpha_{x,y}/2)$. Hence,

$$\varepsilon_{0,\theta}(x, y) = \max\{l_x(\theta), l_y(\theta)\} > \max\{l_x, l_y\} = \varepsilon_{0,\pi/2}(x, y). \tag{5.18}$$

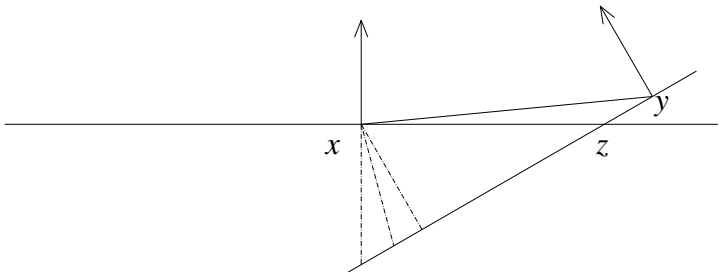

Figure 25. The case of $\alpha_{x,y} < \pi/2$ and $\varphi_{x,y} \in (3\pi/2, 3\pi/2 + \alpha_{x,y})$.

10) $\varphi_{x,y} \in (3\pi/2 + \alpha_{x,y}, 2\pi)$ (see Figure 26). Now, $l_x < l_y$. Because the center of $C_{x,y,z}$ is in the exterior of the triangle Δxyz, we have

$$l_x(\theta) < l_x, l_y(\theta) < l_y, l_x(\theta) < l_y(\theta), \tag{5.19}$$

when $\theta \in (0, \varphi_{x,y} - 3\pi/2 - \alpha_{x,y})$. Hence,

$$\varepsilon_{0,\theta}(x, y) = l_y(\theta) < l_y = \varepsilon_{0,\pi/2}(x, y). \tag{5.20}$$

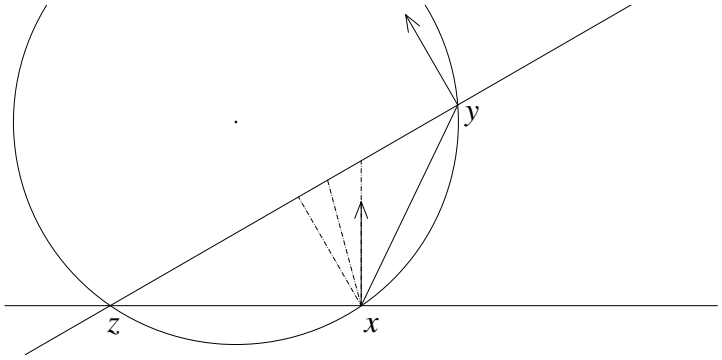

Figure 26. The case of $\alpha_{x,y} < \pi/2$ and $\varphi_{x,y} \in (3\pi/2 + \alpha_{x,y}, 2\pi)$.

Next, assume that $\alpha_{x,y} > \pi/2$.

1) $\varphi_{x,y} \in (\alpha_{x,y} - \pi/2, \alpha_{x,y}/2)$ (see Figure 27). Now, $l_x < l_y$. Because the center of $C_{x,y,z}$ is in the exterior of the triangle Δxyz, we have

$$l_x(\theta) < l_x, l_y < l_y(\theta), l_x(\theta) < l_y(\theta), \tag{5.21}$$

when $\theta \in (0, \varphi_{x,y} + \pi/2 - \alpha_{x,y})$. Hence,

$$\varepsilon_{0,\theta}(x, y) = l_y(\theta) > l_y = \varepsilon_{0,\pi/2}(x, y). \tag{5.22}$$

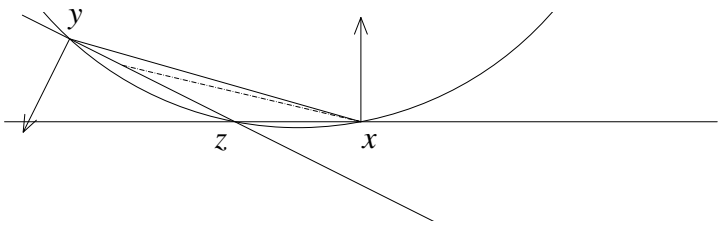

Figure 27. The case of $\alpha_{x,y} > \pi/2$ and $\varphi_{x,y} \in (\alpha_{x,y} - \pi/2, \alpha_{x,y}/2)$.

2) $\varphi_{x,y} \in (\alpha_{x,y}/2, \pi/2)$ (see Figure 28). Now, $l_x > l_y$. Because the center of $C_{x,y,z}$ is in the exterior of the triangle Δxyz, we have

$$l_y < l_y(\theta) < l_x(\theta) < l_x, \tag{5.23}$$

when $\theta \in (0, \varphi_{x,y} - \alpha_{x,y}/2)$. Hence,

$$\varepsilon_{0,\theta}(x, y) = l_x(\theta) < l_x = \varepsilon_{0,\pi/2}(x, y). \tag{5.24}$$

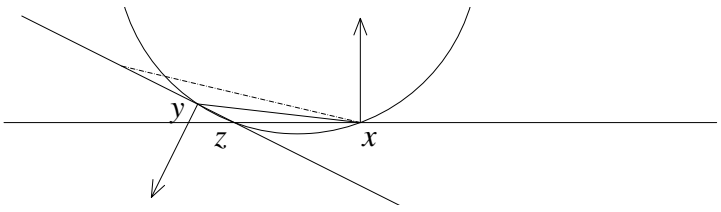

Figure 28. The case of $\alpha_{x,y} > \pi/2$ and $\varphi_{x,y} \in (\alpha_{x,y}/2, \pi/2)$.

3) $\varphi_{x,y} \in (\pi/2, \alpha_{x,y} + \pi/2)$ (see Figure 29). Now,

$$l_x(\theta) < \max\{l_x, l_y\}, l_y(\theta) < \max\{l_x, l_y\}, \tag{5.25}$$

when $\theta \in (0, \alpha_{x,y})$. Hence,

$$\varepsilon_{0,\theta}(x, y) = \max\{l_x(\theta), l_y(\theta)\} < \max\{l_x, l_y\} = \varepsilon_{0,\pi/2}(x, y). \tag{5.26}$$

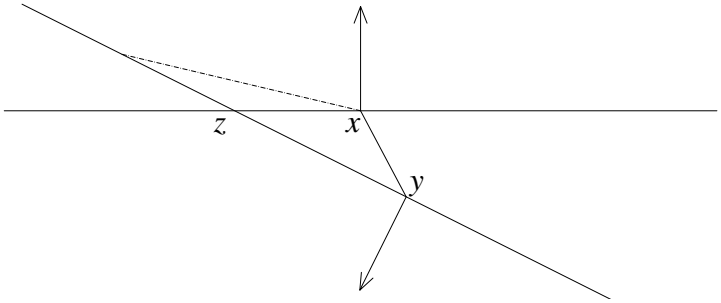

Figure 29. The case of $\alpha_{x,y} > \pi/2$ and $\varphi_{x,y} \in (\pi/2, \alpha_{x,y} + \pi/2)$.

4) $\varphi_{x,y} \in (\alpha_{x,y} + \pi/2, \alpha_{x,y}/2 + \pi)$ (see Figure 30). Now, $l_x < l_y$. Because the center of $C_{x,y,z}$ is in the exterior of the triangle Δxyz, we have

$$l_x < l_x(\theta) < l_y(\theta) < l_y, \tag{5.27}$$

when $\theta \in (0, \pi + \alpha_{x,y}/2 - \varphi_{x,y})$. Hence,

$$\varepsilon_{0,\theta}(x, y) = l_y(\theta) < l_y = \varepsilon_{0,\pi/2}(x, y). \tag{5.28}$$

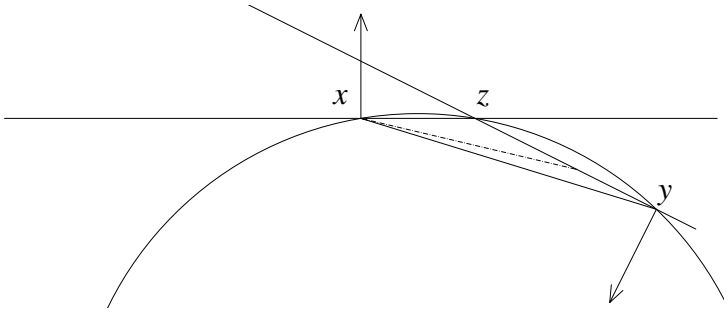

Figure 30. The case of $\alpha_{x,y} > \pi/2$ and $\varphi_{x,y} \in (\alpha_{x,y} + \pi/2, \alpha_{x,y}/2 + \pi)$.

5) $\varphi_{x,y} \in (\alpha_{x,y}/2 + \pi, 3\pi/2)$ (see Figure 31). Now, $l_x > l_y$. Because the center of $C_{x,y,z}$ is in the exterior of the triangle Δxyz, we have

$$l_x < l_x(\theta), l_y(\theta) < l_y, l_y(\theta) < l_x(\theta), \tag{5.29}$$

when $\theta \in (0, 3\pi/2 - \varphi_{x,y})$. Hence,

$$\varepsilon_{0,\theta}(x, y) = l_x(\theta) > l_x = \varepsilon_{0,\pi/2}(x, y). \tag{5.30}$$

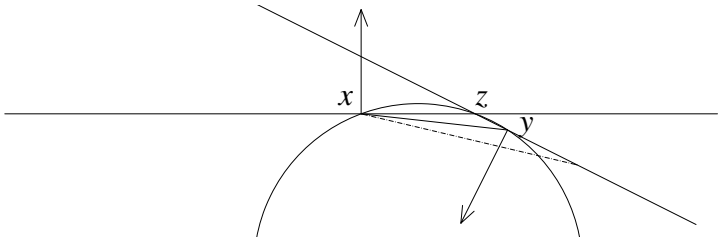

Figure 31. The case of $\alpha_{x,y} > \pi/2$ and $\varphi_{x,y} \in (\alpha_{x,y}/2 + \pi, 3\pi/2)$.

6) $\varphi_{x,y} \in (3\pi/2, \alpha_{x,y} + 3\pi/2)$ (see Figure 32). Now,

$$l_x < l_x(\theta), l_y < l_y(\theta), \tag{5.31}$$

when $\theta \in (0, \pi/2 - \alpha_{x,y}/2)$. Hence,

$$\varepsilon_{0,\theta}(x, y) = \max\{l_x(\theta), l_y(\theta)\} > \max\{l_x, l_y\} = \varepsilon_{0,\pi/2}(x, y). \tag{5.32}$$

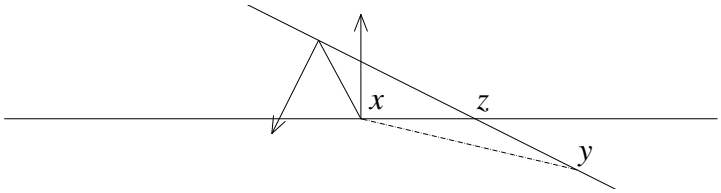

Figure 32. The case of $\alpha_{x,y} > \pi/2$ and $\varphi_{x,y} \in (3\pi/2, \alpha_{x,y} + 3\pi/2)$.

□

6. Discussion

While the wing complex exhibits some advantages, there are several questions left to be addressed:

1) We have focused on analyzing simple curves in $\mathbb{R}^2$, as the geometric structure of curves in two dimensions is relatively simple, making them easier to analyze and validate. However, the situation becomes much more complicated in higher dimensions. For example, in $\mathbb{R}^3$, we must not only consider the curvature variations of points but also the local geometric features of surfaces. Therefore, for the simplicity of theoretical proof, our current work is limited to $\mathbb{R}^2$.
2) For the sake of simplicity in the proof, the theoretical results in this paper are limited to the case $q = 0$, and the framework for arbitrary values of q remains to be further developed. It should be emphasized that, under accurate sampling, the conclusions regarding wing complexes when $q = 0$ are reasonable. In future work, we aim to extend the theoretical proofs to arbitrary values of q.

The introduction of the wing complex opens up new possibilities for persistent homology, especially in data involving curves and manifolds, where local geometric features play a crucial role, making it highly meaningful to capture them through wing complexes. In future work, we plan to focus on

the following directions. First, we will explore the potential of wing complexes in machine learning by designing a dynamic module capable of automatically adjusting the angular parameter θ based on curvature changes, thereby enhancing the adaptability of the wing complex in various geometric scenarios. Next, we plan to extend the concept of wing complexes to three-dimensional space and apply them to 3D point cloud classification and segmentation tasks. Leveraging their ability to adapt to variations in surface curvature, this approach aims to assist in the delineation of boundary regions.

7. Conclusions

In this paper, we introduce wing complexes as a novel method for persistent homology, particularly suited for finite point sets sampled from smooth plane curves. Unlike Čech complexes, our complexes are based on the intersection of wings instead of balls. The key innovation of the wing complex lies in the adjustment of parameter q, which is tuned along the tangent and normal directions to adapt to the local curvature changes of data.

The main contributions of this work are as follows. First, we formally define the wing complex as a new type of simplicial complex and demonstrate its construction. Second, we establish a series of theorems to investigate the relationship between the wing complex and its angular parameters. Third, building on these theoretical results, we analyze the topological properties of wing complexes associated with specific types of curves. Our experiments demonstrate that, compared to the traditional Rips complex construction, the wing complex provides more persistent and accurate topological features. Specifically, wing complexes excel in regions with rapidly changing curvatures, whereas traditional methods may fail to capture the underlying topology correctly.

Author contributions

Zishan Weng: Conceptualization, Methodology, Software, Visualization, Writing–original draft, Writing–review & editing; Minghui Zhao: Conceptualization, Methodology, Supervision, Validation, Funding acquisition, Writing–review & editing. All authors of this article have contributed equally. All authors have read and agreed to the published version of the manuscript.

Use of Generative-AI tools declaration

The authors declare they have not used Artificial Intelligence (AI) tools in the creation of this article.

Acknowledgments

This research has been supported by the National Natural Science Foundation of China (No. 11701028).

Conflict of interest

The authors declare no conflict of interest.

References

1. H. Edelsbrunner, D. Letscher, A. Zomorodian, Topological persistence and simplification, *Discrete Comput. Geom.*, **28** (2002), 511–533. https://doi.org/10.1007/s00454-002-2885-2
2. A. Zomorodian, G. Carlsson, Computing persistent homology, *Discrete Comput. Geom.*, **33** (2005), 249–274. https://doi.org/10.1007/s00454-004-1146-y
3. G. Carlsson, Topology and data, *Bull. Amer. Math. Soc.*, **46** (2009), 255–308. https://doi.org/10.1090/S0273-0979-09-01249-X
4. G. Carlsson, Topological pattern recognition for point cloud data, *Acta Numer.*, **23** (2014), 289–368. https://doi.org/10.1017/S0962492914000051
5. F. Chazal, V. de Silva, S. Oudot, Persistence stability for geometric complexes, *Geom. Dedicata*, **173** (2014), 193–214. https://doi.org/10.1007/s10711-013-9937-z
6. F. Chazal, V. de Silva, M. Glisse, S. Oudot, *The structure and stability of persistence modules*, Cham: Springer, 2016. https://doi.org/10.1007/978-3-319-42545-0
7. Y. Lee, S. D. Barthel, P. Dłotko, S. M. Moosavi, K. Hess, B. Smit, Quantifying similarity of pore-geometry in nanoporous materials, *Nat. Commun.*, **8** (2017), 15396. https://doi.org/10.1038/ncomms15396
8. M. Dindin, Y. Umeda, F. Chazal, Topological data analysis for arrhythmia detection through modular neural networks, In: *Advances in artificial intelligence*, Cham: Springer, 2020, 177–188. https://doi.org/10.1007/978-3-030-47358-7_17
9. M. Carrière, R. Rabadán, Topological data analysis of single-cell hi-c contact maps, In: *Topological data analysis*, Cham: Springer, 2020, 147–162. https://doi.org/10.1007/978-3-030-43408-3_6
10. W. Liu, H. Guo, W. Zhang, Y. Zang, C. Wang, J. Li, Toposeg: topology-aware segmentation for point clouds, In: *Proceedings of the thirty-first international joint conference on artificial intelligence*, 2022, 1201–1208. https://doi.org/10.24963/ijcai.2022/168
11. K. He, J. Shi, H. Fang, Bifurcation and chaos analysis of a fractional-order delay financial risk system using dynamic system approach and persistent homology, *Math. Comput. Simulat.*, **223** (2024), 253–274. https://doi.org/10.1016/j.matcom.2024.04.013
12. R. Brüel-Gabrielsson, B. J. Nelson, A. Dwaraknath, P. Skraba, L. J. Guibas, G. Carlsson, A topology layer for machine learning, arXiv:1905.12200. https://doi.org/10.48550/arXiv.1905.12200
13. M. Ferri, I. Stanganelli, Size functions for the morphological analysis of melanocytic lesions, *Int. J. Biomed. Imaging*, **2010** (2010), 621357. https://doi.org/10.1155/2010/621357
14. S. Y. Oudot, *Persistence theory: from quiver representations to data analysis*, American Mathematical Society, 2015. http://doi.org/10.1090/surv/209
15. F. Chazal, B. Michel, An introduction to topological data analysis: fundamental and practical aspects for data scientists, *Front. Artif. Intell.*, **4** (2021), 667963. https://doi.org/10.3389/frai.2021.667963
16. S. Dantchev, I. Ivrissimtzis, Efficient construction of the Čech complex, *Comput. Graph.*, **36** (2012), 708–713. https://doi.org/10.1016/j.cag.2012.02.016

17. A. Zomorodian, Fast construction of the Vietoris-Rips complex, *Comput. Graph.*, **34** (2010), 263–271. https://doi.org/10.1016/j.cag.2010.03.007

18. C. Maria, J.-D. Boissonnat, M. Glisse, M. Yvinec, The gudhi library: simplicial complexes and persistent homology, In: *Mathematical software—ICMS 2014*, Berlin, Heidelberg: Springer, 2014, 167–174. https://doi.org/10.1007/978-3-662-44199-2_28

19. G. Tauzin, U. Lupo, L. Tunstall, J. B. Pérez, M. Caorsi, A. M. Medina-Mardones, et al., giotto-tda: A topological data analysis toolkit for machine learning and data exploration, *J. Mach. Learn. Res.*, **22** (2021), 1–6.

20. H. Edelsbrunner, E. P. Mücke, Three-dimensional alpha shapes, *ACM Transactions On Graphics (TOG)*, **13** (1994), 43–72. https://doi.org/10.1145/174462.156635

21. V. de Silva, G. E. Carlsson, Topological estimation using witness complexes, In: *Eurographics Symposium on Point-Based Graphics*, 2004, 157–166. https://doi.org/10.2312/SPBG/SPBG04/157-166

22. P. Breiding, S. Kališnik, B. Sturmfels, M. Weinstein, Learning algebraic varieties from samples, *Rev. Mat. Complut.*, **31** (2018), 545–593. https://doi.org/10.1007/s13163-018-0273-6

23. S. Kališnik, D. Lešnik, Finding the homology of manifolds using ellipsoids, *Journal of Applied and Computational Topology*, **8** (2024), 193–238. https://doi.org/10.1007/s41468-023-00145-6

24. N. Canova, S. Kališnik, A. Moser, B. Rieck, A. Žegarac, Persistent homology via ellipsoids, arXiv:2408.11450. https://doi.org/10.48550/arXiv.2408.11450

25. A. Hatcher, *Algebraic topology*, Cambridge University Press, 2002.

26. M. B. Botnan, Topological data analysis, 2024. Available from: `https://www.few.vu.nl/~botnan/lecture_notes.pdf`.

27. U. Bauer, M. Kerber, F. Roll, A. Rolle, A unified view on the functorial nerve theorem and its variations, *Expo. Math.*, **41** (2023), 125503. https://doi.org/10.1016/j.exmath.2023.04.005

AIMS Press